High-temperature expansions for the J_1-J_2 Heisenberg models: Applications to *ab initio* calculated models for Li_2VOSiO_4 and Li_2VOGeO_4

H. Rosner,[1,*] R. R. P. Singh,[1] W. H. Zheng,[2] J. Oitmaa,[2] and W. E. Pickett[1]
[1]*Department of Physics, University of California, Davis, California 95616*
[2]*School of Physics, University of New South Wales, Sydney, New South Wales 2052, Australia*
(Received 17 May 2002; revised manuscript received 14 October 2002; published 22 January 2003)

We develop high-temperature expansions for the uniform susceptibility and specific heat of the square-lattice J_1-J_2 Heisenberg models. Combined with a perturbative mean-field theory, we obtain accurate results for the uniform susceptibility of the large-J_2/J_1 Heisenberg model at all temperatures. For the specific heat, the high-temperature expansions show good convergence down to the peak temperature, where the specific heat has a maximum. Exchange couplings are calculated for Li_2VOSiO_4 (Li_2VOGeO_4) using local-density approximation (LDA) and found to be $J_1=0.75$ K (1.7 K), $J_2=8.8$ K (8.1 K), and $J_\perp=0.25$ K (0.19 K), respectively. Using the high-temperature expansion results, we show that the specific heat and uniform susceptibility of these materials are well described by a large-J_2/J_1 Heisenberg model in agreement with the LDA predictions. Furthermore, the measured Néel temperature is consistent with our LDA derived $J_\perp$ values. Further experiments which would be particularly suited to an accurate determination of the J_2/J_1 ratio for these systems are discussed.

DOI: 10.1103/PhysRevB.67.014416 PACS number(s): 75.10.Jm, 71.15.Mb, 75.30.Et

I. INTRODUCTION

Frustrated square-lattice spin-1/2 Heisenberg antiferromagnets with Hamiltonian

$$H_{spin}=\sum_{ij} J_{ij}\vec{S}_i\vec{S}_j, \tag{1}$$

with nearest-neighbor exchange J_1 and second-neighbor (diagonal) exchange J_2 have received considerable attention recently.[1,2] Of particular theoretical interest has been the phase diagram of the model as a function of J_2/J_1 and the possibility of a spin-liquid phase at intermediate J_2/J_1. Several results have been established. When J_1 dominates ($J_2/J_1\leqslant 0.3$), the system is Néel ordered. When J_2 dominates ($J_2/J_1\geqslant 0.6$), there are two interpenetrating Néel lattices whose relative alignment is frustrated, and a columnar antiferromagnetic order is selected by quantum fluctuations with wave vector $Q=(\pi,0)$ or $(0,\pi)$.[3–5] In the intermediate regime, almost all numerical studies find a spin-gap phase, but whether one has a true spin liquid or a phase with broken translational symmetry remains a matter of debate.[1,2,6]

Recent discovery of several quasi-two-dimensional (2D) materials, which are realizations of the J_1-J_2 model, has raised the need for accurate theoretical calculations of the thermodynamic properties of these models to compare with experiments, and high-temperature expansions provide the most accurate way to determine these properties. The J_1-J_2 materials include $VOMoO_4$,[7] $Pb_2VO(PO_4)_2$,[8] and especially Li_2VOSiO_4 and Li_2VOGeO_4. These latter two compounds have been reported by Melzi *et al.*,[9,10] who provide data for specific heat, magnetization, NMR, and muon spin rotation. These data provide a reasonably firm value of $J_1+J_2\approx 8$ K; further, these authors suggested a ratio $J_2/J_1\sim 1$ might be appropriate. In a recent report of some of the results of the present paper, Rosner *et al.*[11] presented a reanalysis of the data spurred by *ab initio* estimates of J_2 and J_1 which gave much larger J_2/J_1 values.

The primary objective of this paper is to extend knowledge of the behavior of the J_1-J_2 model (through high-temperature expansions) and thereby to provide detailed quantitative understanding of the magnetic properties of the materials Li_2VOSiO_4 and Li_2VOGeO_4. These compounds are layered spin systems that are well described by the ionic picture, leaving V^{4+} ions with the d^1, $S=\frac{1}{2}$ moments whose interactions within the layer are much stronger than between layers, thus providing a good representation of the J_1-J_2 model. This paper provides the full analysis and some extension of the recent report of Rosner *et al.*[11] To address the behavior of this system, high-temperature expansions of the thermodynamic properties of this model are presented. We also apply local-density approximation (LDA) calculations to obtain *ab initio* estimates of exchange constants for these materials. These are combined with the results of high-temperature expansions to investigate the susceptibility and specific heat. Although these thermodynamic properties are not very sensitive to the J_2/J_1 ratio, they still suffice to rule out certain parameter ranges. Comparison with experimental data shows that these materials are good realizations of large J_2/J_1 model in agreement with the LDA derived values.

The plan of the paper is as follows. In Sec. II, we discuss the high-temperature expansions for the J_1-J_2 model, and then we discuss a perturbative mean-field theory, valid for small J_1/J_2, which allows us to get accurate numerical values for the uniform susceptibility of the model at all temperatures. In Sec. III, we present the LDA calculations for the materials Li_2VOSiO_4 and Li_2VOGeO_4. A two-band tight-binding (TB) model is fitted to the LDA band structure, and mapped onto a Heisenberg model with in-plane (J_1 and J_2) and interplane ($J_\perp$) exchange constants.

In Sec. IV, we present comparisons of the experimental data for uniform susceptibility and specific heat with our

TABLE I. Series coefficients for the high-temperature expansions of the uniform susceptibility $\chi(T)=T^{-1}\Sigma_n\beta_1^n\Sigma_m c_{m,n}x^m$ and the internal energy $U(T)=\Sigma_n\beta_1^n\Sigma_m e_{m,n}x^m$, where $\beta_1=J_1/k_BT$ and $x=J_2/J_1$. Nonzero coefficients $c_{m,n}$ up to order $n=9$ are listed.

$\chi(T)$							
(m,n)	$c_{m,n}$	(m,n)	$c_{m,n}$	(m,n)	$c_{m,n}$	(m,n)	$c_{m,n}$
(0,0)	2.500000000×10^{-1}	(4,4)	1.692708333×10^{-2}	(0,7)	6.285652282×10^{-4}	(6,8)	1.827756851×10^{-1}
(0,1)	$-2.500000000\times10^{-1}$	(0,5)	$-9.244791667\times10^{-3}$	(1,7)	$-1.069335937\times10^{-2}$	(7,8)	1.761222718×10^{-2}
(1,1)	$-2.500000000\times10^{-1}$	(1,5)	$-4.427083333\times10^{-2}$	(2,7)	$-1.265679253\times10^{-1}$	(8,8)	3.978426494×10^{-4}
(0,2)	1.250000000×10^{-1}	(2,5)	$-1.575520833\times10^{-1}$	(3,7)	1.852756076×10^{-3}	(0,9)	$-5.211347415\times10^{-4}$
(1,2)	5.000000000×10^{-1}	(3,5)	$-5.625000000\times10^{-1}$	(4,7)	$-3.238661024\times10^{-1}$	(1,9)	$-3.002978128\times10^{-3}$
(2,2)	1.250000000×10^{-1}	(4,5)	$-1.796875000\times10^{-1}$	(5,7)	$-3.126790365\times10^{-1}$	(2,9)	5.435229105×10^{-2}
(0,3)	$-4.166666667\times10^{-2}$	(5,5)	$-9.244791667\times10^{-3}$	(6,7)	$-4.634331597\times10^{-2}$	(3,9)	$-1.319648056\times10^{-1}$
(1,3)	$-3.437500000\times10^{-1}$	(0,6)	1.991102431×10^{-3}	(7,7)	6.285652282×10^{-4}	(4,9)	$-1.452223520\times10^{-1}$
(2,3)	$-5.000000000\times10^{-1}$	(1,6)	4.973958333×10^{-2}	(0,8)	3.978426494×10^{-4}	(5,9)	1.101984902×10^{-2}
(3,3)	$-4.166666667\times10^{-2}$	(2,6)	4.075520833×10^{-2}	(1,8)	$-1.114095052\times10^{-2}$	(6,9)	$-2.600314993\times10^{-1}$
(0,4)	1.692708333×10^{-2}	(3,6)	2.427951389×10^{-1}	(2,8)	4.545724051×10^{-2}	(7,9)	$-1.012868245\times10^{-1}$
(1,4)	9.895833333×10^{-2}	(4,6)	4.653645833×10^{-1}	(3,8)	1.822102865×10^{-1}	(8,9)	$-5.757359096\times10^{-3}$
(2,4)	5.234375000×10^{-1}	(5,6)	9.401041667×10^{-2}	(4,8)	$-3.278421069\times10^{-2}$	(9,9)	$-5.211347415\times10^{-4}$
(3,4)	3.333333333×10^{-1}	(6,6)	1.991102431×10^{-3}	(5,8)	3.302366226×10^{-1}		
$U(T)$							
(m,n)	$e_{m,n}$	(m,n)	$e_{m,n}$	(m,n)	$e_{m,n}$	(m,n)	$e_{m,n}$
(0,1)	$-3.750000000\times10^{-1}$	(0,5)	$-6.347656250\times10^{-3}$	(1,7)	1.388020833×10^{-1}	(7,8)	$-2.042149135\times10^{-2}$
(2,1)	$-3.750000000\times10^{-1}$	(1,5)	$-1.734375000\times10^{-1}$	(2,7)	$-3.949102493\times10^{-1}$	(9,8)	8.162507557×10^{-3}
(0,2)	$-9.375000000\times10^{-2}$	(2,5)	4.365234375×10^{-1}	(3,7)	$-6.493675595\times10^{-2}$	(0,9)	3.237876690×10^{-3}
(1,2)	5.625000000×10^{-1}	(3,5)	$-1.953125000\times10^{-2}$	(4,7)	5.989234561×10^{-2}	(1,9)	$-8.633584320\times10^{-2}$
(3,2)	$-9.375000000\times10^{-2}$	(4,5)	$-7.675781250\times10^{-2}$	(5,7)	1.329055060×10^{-2}	(2,9)	2.225171649×10^{-1}
(0,3)	5.468750000×10^{-2}	(6,5)	$-6.347656250\times10^{-3}$	(6,7)	3.964843750×10^{-2}	(3,9)	3.161434597×10^{-1}
(1,3)	1.250000000×10^{-1}	(0,6)	$-2.113444010\times10^{-2}$	(8,7)	$-2.788144066\times10^{-3}$	(4,9)	$-3.155230164\times10^{-1}$
(2,3)	$-1.562500000\times10^{-1}$	(1,6)	1.266927083×10^{-1}	(0,8)	8.162507557×10^{-3}	(5,9)	$-6.515987336\times10^{-2}$
(4,3)	5.468750000×10^{-2}	(2,6)	1.895833333×10^{-1}	(1,8)	$-2.938842773\times10^{-2}$	(6,9)	1.191482140×10^{-1}
(0,4)	4.882812500×10^{-2}	(3,6)	$-2.053059896\times10^{-1}$	(2,8)	$-3.086124965\times10^{-1}$	(7,9)	$-2.493560630\times10^{-3}$
(1,4)	$-3.125000000\times10^{-1}$	(4,6)	$-1.925455729\times10^{-2}$	(3,8)	4.990875244×10^{-1}	(8,9)	$-2.928678321\times10^{-2}$
(2,4)	$-1.953125000\times10^{-2}$	(5,6)	7.097981771×10^{-2}	(4,8)	2.152143206×10^{-2}	(10,9)	3.237876690×10^{-3}
(3,4)	$-5.859375000\times10^{-2}$	(7,6)	$-2.113444010\times10^{-2}$	(5,8)	$-1.450156076\times10^{-1}$		
(5,4)	4.882812500×10^{-2}	(0,7)	$-2.788144066\times10^{-3}$	(6,8)	1.131243025×10^{-2}		

calculations. In Sec. V, we discuss the observed Néel temperature for the material and relate it to LDA calculated interplane couplings. In Sec. VI, we discuss some aspects of the spin-wave spectra for the J_1-J_2 model, which are sensitive to the J_1/J_2 ratio, and can thus be used for accurate experimental determination of these ratios. We summarize in Sec. VII.

II. THEORETICAL TREATMENT OF THE J_1-J_2 MODEL

A. High-temperature expansions

Using cluster expansion methods,[12] high-temperature series expansions are developed for the uniform susceptibility and the internal energy of the J_1-J_2 model for arbitrary values of J_1/J_2. Let $\beta_1=J_1/k_BT$ and $x=J_2/J_1$. We write the uniform susceptibility expansion as

$$T\chi=\sum_n \beta_1^n \sum_m c_{m,n}x^m, \tag{2}$$

and the internal energy expansion as

$$U=\sum_n \beta_1^n \sum_m e_{m,n}x^m. \tag{3}$$

The coefficients $c_{m,n}$ and $e_{m,n}$ complete to order $n=9$ are presented in Table I. The specific heat is obtained by the relation

$$C=dU/dT.$$

To obtain numerical estimates of the uniform susceptibility and specific heat for a given value of J_1/J_2, we first obtain a single variable series in inverse temperature. Since in this paper, we are most interested in small J_1/J_2 ratios, the single variable series coefficients are obtained in the variable J_2/k_BT. These series are extrapolated beyond their radius of convergence using Pade and differential approximants.[13]

B. Perturbative Mean-field theory and low-temperature susceptibility

High-temperature expansions provide essentially exact numerical values for the thermodynamic properties at high-temperatures. However, below a certain temperature, their convergence necessarily becomes poor. In this section, we discuss how the knowledge of the uniform susceptibility for the nearest-neighbor Heisenberg model, together with a perturbative mean-field theory, can lead to accurate estimates for the uniform susceptibility of the small J_1/J_2 Heisenberg model at all temperatures.

Using series expansions ($T=0$),[14] nonlinear sigma model theory[15] (very low T), quantum Monte Carlo (QMC) simulations[16] (low T) and high-temperature expansions (HTE) (high T),[17] the susceptibility of the nearest-neighbor model ($J_1=0$) is known accurately for all T. We treat the J_1 term perturbatively,[18] and set $J_2=1$ for notational simplicity. Due to strong frustration, the large J_2 model appears as two disconnected interpenetrating antiferromagnets. The application of a field causes a uniform polarization of both the sublattices. These polarized moments will now interact through antiferromagnetic J_1 leading to a suppression of the polarized moment. To see the perturbative calculation, we write the Hamiltonian as

$$\mathcal{H}=\mathcal{H}_0+J_1\sum_{ij}\vec{S}_i\vec{S}_j-h\sum_i S_i^z, \tag{4}$$

where $\mathcal{H}_0$ is the Hamiltonian for $J_1=0$ and we have included the external field term explicitly. In treating the J_1 term perturbatively, note that the spins on the two sublattices are decoupled without J_1 and hence for spins on the two sublattices $\langle S_iS_j\rangle=\langle S_i\rangle\langle S_j\rangle$. This leads to the following expression for the free energy per site f to first order in J_1 and second order in h:

$$f=f_0-\tfrac{1}{2}\chi_0h^2+2J_1m_0^2=f_0-\tfrac{1}{2}\chi_0h^2+2J_1\chi_0^2h^2. \tag{5}$$

Here, f_0 and χ_0 are the free energy and susceptibility per site for $J_1=0$ (a nearest-neighbor Heisenberg model). From this, it follows that

$$\chi(J_1,T)=\chi_0(T)[1-4J_1\chi_0(T)]. \tag{6}$$

As shown in the inset of Fig. 1, at $T=0$ for small J_1/J_2, this expression compares very well with the perpendicular susceptibility $\chi_\perp$ calculated from Ising series expansions.[14] Note that the perpendicular susceptibility $\chi_\perp$ is equal to 2/3 of uniform susceptibility $\chi(T)$ at $T=0$. Figure 1 also shows that applying Eq. (6) to the finite-T QMC data for χ_0 leads to susceptibility values, which join smoothly with the high-temperature expansion results. Thus, we have accurate calculations for the susceptibility of the model with small J_1/J_2 at all T.

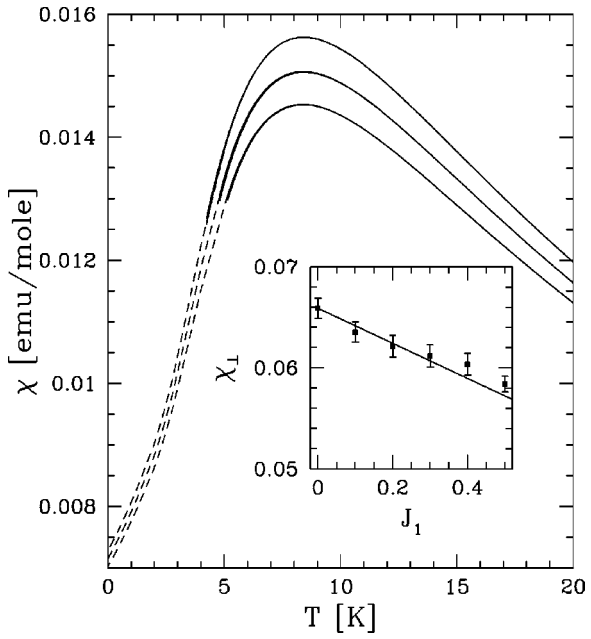

FIG. 1. Susceptibility (χ, with largest χ for $J_1=0$) for $J_2=9$ K, $g=2$, and $J_1/J_2=0,0.1,0.2$. The low-temperature data is obtained from QMC combined with Eq. (6), while the high-temperature data comes from HTE. The inset shows the perpendicular susceptibility $\chi_\perp$ for $T=0,J_2=1$ calculated from Ising series expansion (points with errorbar) and from Eq. (6) (solid line).

III. LDA CALCULATIONS FOR Li_2VOSiO_4 AND Li_2VOGeO_4

A. Crystal structure

The isostructural compounds Li_2VOSiO_4 and Li_2VOGeO_4 crystallize in the tetragonal $P4/nmm$ system containing two formula units per cell with $a=6.3682$ Å, $c=4.449$ Å for Li_2VOSiO_4 and $a=6.4779$ Å, $c=4.520$ Å for Li_2VOGeO_4.[19] A sketch of the crystal structure is shown in Fig. 2. The magnetically active network of spin-1/2 V^{4+} ions is built up by $[VOSi(Ge)O_4]^{2-}$ layers of VO_5 square pyramids sharing its four vertices with $Si(Ge)O_4$ tetrahedra. These complex layers are ''intercalated'' stoichiometrically with Li ions. The structure of the V^{4+} square network suggests that both the nearest-neighbor (NN) and the next-nearest-neighbor (NNN) in-plane coupling should be significant, although it is at best difficult to decide from general considerations whether one is dominant, or even which one might be largest. The NN coupling is favored by the existence of two exchange channels and shorter distance, the NNN coupling profits from a straighter connection between pyramids oriented in the same direction forming a planar V^{4+} network (see Fig. 2). The magnetically active V^{4+} ions have the site symmetry $4mm$, leading to a splitting of the V $3d$ states into four levels, preserving only the degeneracy of the V $3d_{xz}$ and $3d_{yz}$ states.

B. Calculational method

Scalar relativistic band-structure calculations were performed using the full-potential nonorthogonal local-orbital

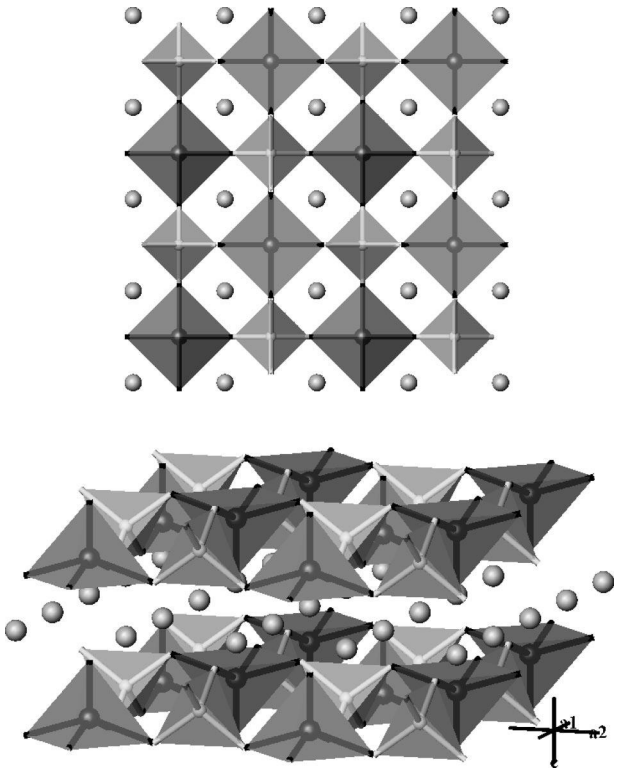

FIG. 2. Perspective view (lower panel) of the crystal structure of Li_2VOSiO_4, and projection along [001] (upper panel). The VO_5 pyramids (large diamonds) share the corners of the basal planes with SiO_4 tetrahedra (small diamonds). The V^{4+} and Si^{4+} ions are represented by black and gray spheres with bonds to the oxygens located at the corners of the pyramids and tetrahedra, respectively. The Li^+ ions are indicated by medium sized gray spheres. In the isostructural Li_2VOGeO_4, Si is replaced by Ge.

minimum-basis scheme[20] within the LDA to obtain the hopping part of a TB Hamiltonian. For the exchange and correlation potential, the parametrization of Perdew and Zunger[21] was used. V($3s$,$3p$,$4s$,$4p$,$3d$), O($2s$,$2p$,$3d$), Li($2s$,$2p$), Si($3s$,$3p$,$3d$), and Ge($3d$,$4s$,$4p$,$4d$) states, respectively, were chosen as the basis set. All states lying lower were treated as core states. The inclusion of V($3s$,$3p$) and Ge $3d$ states in the valence states was necessary to account for nonnegligible core-core overlaps due to the relatively large extension of the V ($3s$,$3p$) and Ge $3d$ wave functions. The O and Si $3d$, Ge $4d$, as well as the Li $2p$ states were taken into account to get a more complete basis set. The spatial extension of the basis orbitals, controlled by a confining potential[22] $(r/r_0)^4$, was optimized to minimize the total energy. A k mesh of 432 points in the Brillouin zone (70 in the irreducible part) was used. Convergence with respect to the basis set and the k mesh was carefully checked.

C. Electronic structure

The nonpolarized energy bands are very similar for these compounds. We find in both cases a valence-band complex of about 10 eV width with two bands crossing the Fermi level. Figure 3 shows the total and partial density of states

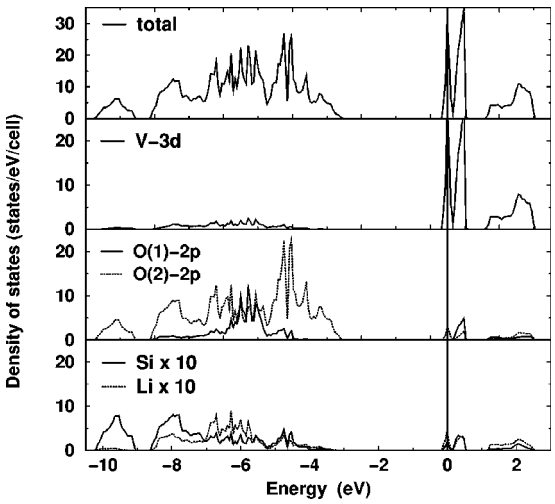

FIG. 3. Total and partial density of states of Li_2VOSiO_4. The Fermi level is at zero energy. O(2) stands for the O atom in the basal plane of the VO_5 pyramids, O(1) sits at the top of the pyramids. Note that the Si and Li states are scaled by a factor of 10.

(DOS) for Li_2VOSiO_4. Typical of vanadates, the valence band has predominantly O $2p$ character, with some admixture of V and small contributions from Li and Si (note that the partial DOS in Fig. 3 for Li and Si is scaled by a factor of 10). The states at and right above the Fermi level are built primarily from V $3d$ orbitals, with the dispersion arising from hybridization with the O $2p$ states, and with practically negligible admixture of Li and Si states. The isostructural and isovalent replacement of Ge for Si in Li_2VOGeO_4 leads to a virtually identical picture on the energy scale shown in Fig. 3. The ionic picture $Li_2^{1+}V^{4+}O^{2-}Si^{4+}(Ge^{4+})O_4^{2-}$ provides an excellent overall picture of the electronic structure.

The two bands crossing the Fermi level, due to the two V^{4+} ions per cell, are well separated by a gap of about 3 eV from the rest of the valence-band complex. These relatively narrow bands (see Fig. 4, left panel) are half filled. Therefore, strong correlation effects can be expected, which explain the experimentally observed insulating ground state. The half-filled bands show mainly V $3d_{xy}$ (see Fig. 4, right

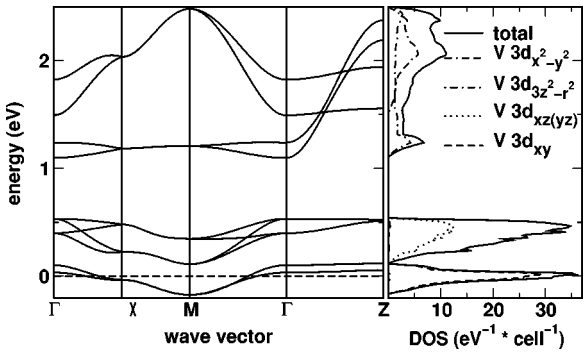

FIG. 4. Band structure (left panel), and orbital-resolved DOS of Li_2VOSiO_4 for the V $3d$ related bands. The Fermi level is at zero energy. The notation of the symmetry points is as follows: $X=(100)$, $M=(110)$, $Z=(001)$.

TABLE II. Transfer integrals of the two-band TB model for Li_2VOSiO_4 and the corresponding exchange couplings for different values of the Hubbard U. The corresponding values for Li_2VOGeO_4 are given in parentheses.

t_1 (meV)	t_2 (meV)	$t_\perp$ (meV)	U (eV)	J_1 (K)	J_2 (K)	$J_\perp$ (K)
8.5	29.1	−4.8	4	0.83	9.81	0.27
(12.8)	(28.0)	(−4.1)		(1.88)	(9.07)	(0.20)
			5	0.67	7.85	0.22
				(1.52)	(7.26)	(0.16)

panel) and minor O(2) $2p_{x,y}$ character (oxygens of the basal plane of the VO_5 pyramid) in the analysis of the corresponding orbital-resolved partial densities of states (not shown for O). The band complex of four bands about 0.4 eV above the Fermi level is due to V $3d_{xz}$ and $3d_{yz}$ states (see Fig. 4, right panel) and shows negligible mixing with the half-filled bands. Thus, the LDA picture is that, relative to the singly occupied d_{xy} orbital, there is a crystal-field splitting of the d_{xz},d_{yz} to 0.4 eV higher energy, with the remaining two orbitals $\sim$1.5 eV higher than the d_{xy} state and broadened by interlayer dispersion. (Of course, correlation effects will shift the positions of the half-filled state.) The differences between Li_2VOSiO_4 and Li_2VOGeO_4 are rather small, the main difference is a slightly larger splitting of the V $3d_{xy}$ derived bands along the Γ-X line for the latter compound, resulting in an increased NN transfer integral.

Because the low-lying magnetic excitations involve only those orbitals with unpaired spins (corresponding to the two half-filled bands) and because of the negligible mixing of these states with other bands close to the Fermi level, we restrict ourselves to a two-band TB analysis and the discussion of these half-filled bands.

D. Tight binding representation

The dispersion of these bands can be represented in 2 $\times$2 form (see Fig. 4) in terms of NN transfer t_1 and NNN transfer t_2 within the [001] plane (see Fig. 2, upper panel) and NN hopping $t_\perp$ between neighboring planes as

$$E(\vec{k}) = \varepsilon_0 + 2t_2[\cos(k_x a) + \cos(k_y b)] \pm 4t_1 \cos(k_x a/2)\cos(k_y b/2) + 2t_\perp \cos(k_z c). \quad (7)$$

Parameters have been obtained by two different numerical procedures: by straightforward least-square fitting of the complete pair of bands, and separately by using the energy eigenvalues at selected high-symmetry points. The resulting hopping amplitudes for both compounds are shown in Table II. The uncertainties can be estimated from the differences in the two procedures at about 5% for the in-plane transfers and 15% for the interplane term from the differences of the above-mentioned fitting procedures. These small differences can be ascribed to the influence of longer-range interactions, which we neglect. The agreement of the TB fit with the LDA bands justifies *a posteriori* the restriction to NN and NNN couplings only. Comparing the transfer integrals (given in Table II) for Li_2VOSiO_4 and Li_2VOGeO_4, the main difference consists of about 50% larger NN term in Li_2VOGeO_4, whereas the NNN hopping and the interplane hopping $t_\perp$ are only slightly smaller than in Li_2VOSiO_4.

E. Calculated exchange coupling

The resulting transfer integrals enable us to estimate the relevant exchange couplings, crucial for the derivation and examination of magnetic model Hamiltonians of the spin-1/2 Heisenberg type like Eq. (1). In general, the total exchange J can be divided into an antiferromagnetic and a ferromagnetic contribution $J = J^{AFM} + J^{FM}$. In the strongly correlated limit, valid for typical vanadates, the former can be calculated in terms of the one-band extended Hubbard model $J_i^{AFM} = 4t_i^2/(U - V_i)$. The index i corresponds to NN and NNN, U is the on-site Coulomb repulsion and V_i is the intersite Coulomb interaction. Considering the fact that the VO_5 pyramids are not directly connected, but only indirectly via SiO_4 tetrahedra, ferromagnetic contributions J^{FM} are expected to be small and we neglect them. For the same reason, the intersite Coulomb interactions V_i should be negligible compared with the on-site repulsion U. From LDA-DMFT(QMC) studies[23] and by fitting spectroscopic data to model calculations,[24] $U \sim 4$–5 eV is estimated for typical vanadates. Therefore, we adopt $U = 4$ eV and $U = 5$ eV as representative values to estimate the exchange constants and their sensitivity to U. The resulting values for the exchange integrals for both compounds are given in Table II.

Our calculated exchange couplings can be compared with the experimental findings.[10] For Li_2VOSiO_4, we find excellent agreement for the sum[25] $J_1 + J_2 = 9.5 \pm 1.5$ K of the in-plane couplings, reported from susceptibility data[10,9] to be $J_1 + J_2 = 8.2 \pm 1$ K. For Li_2VOGeO_4, we find the same result for the sum $J_1 + J_2$, with changes for both J_1 and J_2 being of the same size with opposite sign (see Table II). Experimentally, the Curie-Weiss temperature in Li_2VOGeO_4 was found to be about 30% smaller than in Li_2VOSiO_4.[9] In sharp contrast to the results of Ref. 10, where they estimate $J_2/J_1 \sim 1.1 \pm 0.1$, we find a ratio $J_2/J_1 \sim 12$, exceeding the experimentally derived ratio by an order of magnitude. Analyzing the uniform susceptibility and the specific heat in Sec. IV, we will show that our result is much more consistent with the experimental data than the estimate $J_2/J_1 \sim 1.1$.[10] Because of more than twice as large NN exchange, J_1 in Li_2VOGeO_4 compared to Li_2VOSiO_4, a ratio $J_2/J_1 \sim 5$ is considerably smaller, but still deep in part of the phase diagram for the columnar ordered phase.

IV. COMPARISONS WITH EXPERIMENTAL DATA: UNIFORM SUSCEPTIBILITY AND SPECIFIC HEAT

The experimental data for susceptibility and specific heat of these materials go from room temperature down to a few Kelvin (below the Néel temperature). Below the 3D, long-range order, one does not expect the 2D models to remain valid. But also at high temperatures these systems do not show a Curie-Weiss regime. Rather, a plot of the inverse susceptibility versus temperature shows a continuously

changing slope, which cannot be accounted for by a Heisenberg model. Our primary focus is on data below 20 K, which still go about twice above the Curie-Weiss temperature.

In our data fitting, we use the same approach as described in detail in Ref. 26. Here, there are three fitting parameters: J_1/J_2, J_2, and g. The basic procedure is to find a proper parameter set $(J_1/J_2, J_2, g)$, which gives the minimum value of

$$P=\sum_{T_i} |\chi^{\rm exp}(T_i)-\chi^{\rm theo}(T_i)|, \tag{8}$$

for susceptibility, or

$$P=\sum_{T_i} |C_v^{\rm exp}(T_i)-C_v^{\rm theo}(T_i)|, \tag{9}$$

for specific heat, where superscripts exp and theo mean the experimental and theoretical results, respectively, and the summation is over the experimental points T_i.

We first consider the data for the material Li_2VOSiO_4. We find that fitting of the susceptibility and specific-heat data is not very sensitive to the J_2/J_1 ratio. If we fit the susceptibility data, allowing the parameters $(J_1/J_2,\ J_2,\ g)$ to vary freely, the best fit is obtained for the parameters (0.45, 5.9 K, 1.97). Note that the best fit for the susceptibility data alone gives a g value very close to 2 in agreement with the value quoted from the electron-spin-resonance measurements by Melzi *et al.*[10] Accepting a g value of 2 will lead to a J_1/J_2 ratio close to one half. If we fit the specific-heat data, the best fit arises for $(J_1/J_2,\ J_2)$ values of (0.025, 5.9 K). In both cases, the fits of J_1/J_2 are strongly correlated with the fits for J_2. Combining the trends for both specific-heat and susceptibility data, the best fit for the materials gives $(J_1/J_2,\ J_2,\ g)$ of (0.3, 5.9 K, 1.93).

In looking for consistency between the LDA calculations and the experimental data, we can adopt the following strategy. In LDA, the ratio of exchange constants should be best determined as the parameter U cancels out. Hence, we fix $J_2/J_1=10$ consistent with LDA. We then vary g and J_2 to obtain the best fit to the susceptibility data. This is obtained for $J_2=6.1$ K, 20% smaller than the lower estimate from the LDA calculation of Sec. III E. The agreement is still remarkable for an *ab initio* calculation.

The data are represented excellently by the susceptibility fit as shown in the upper panel of Fig. 5. The specific-heat data are now compared with theory with *no adjustable parameters*. This is shown in the inset of the figure. The agreement is remarkable. In the middle panel of Fig. 5, we also show the corresponding best fit for $J_1/J_2=0.3$, which shows an even better fit. We also applied the same fitting procedure for $J_2/J_1=1$, the value proposed in Ref. 10. The agreement is poor as shown in the lower panel of Fig. 5. Thus, although the susceptibility and specific-heat data do not allow us to fix the exchange integrals unambiguously, they are quite consistent with small J_1/J_2 ratio as found in LDA, and inconsistent with $J_2\approx J_1$.

We now turn to the material Li_2VOGeO_4. For this material, when we fit the susceptibility data, allowing the parameters $(J_1/J_2,\ J_2,\ g)$ to vary freely, the best fit is obtained for the parameters (0.55, 3.8 K, 1.83). If we fit the specific-heat data, the best fit arises for $(J_1/J_2,\ J_2)$ values of (0.75, 4.1 K). In this case also, the fits of J_1/J_2 are strongly correlated

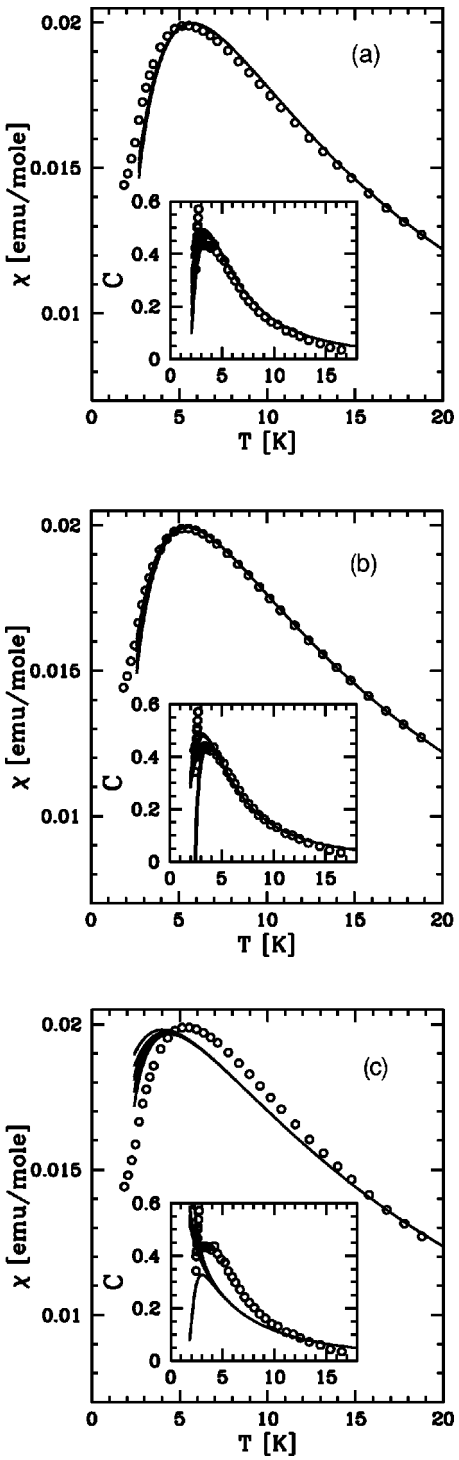

FIG. 5. Susceptibility and specific heat (inset) for Li_2VOSiO_4 compared with the Heisenberg model results for $J_1/J_2=$ (a) 0.1, (b) 0.3 and (c) 1.0. The full lines are the calculated curves, the open circles are the data points according to Refs. 9 and 10. The different curves for the specific heat correspond to different Pade approximations.

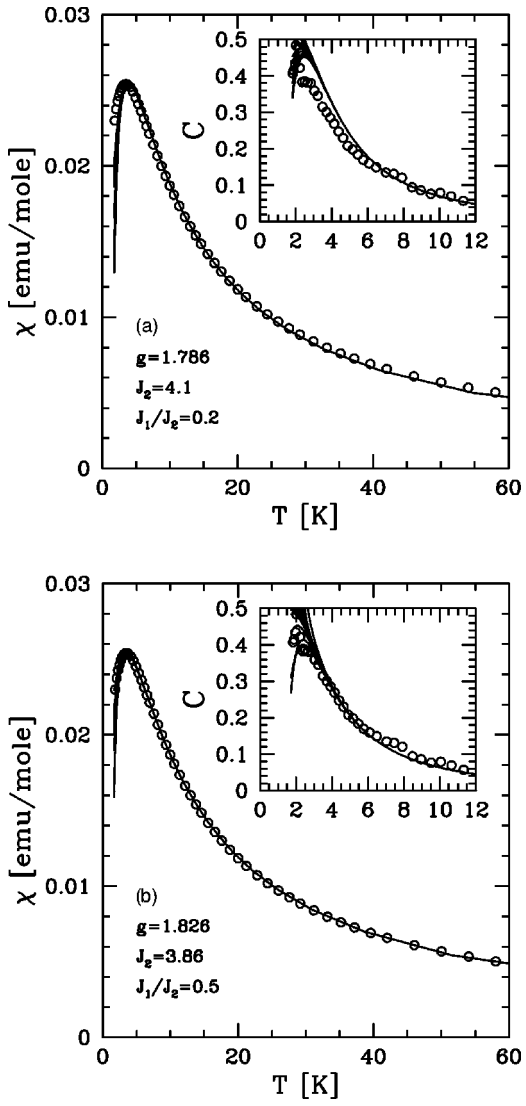

FIG. 6. Susceptibility and specific-heat (inset) for Li_2VOGeO_4 compared with the Heisenberg model results for $J_1/J_2=$(a) 0.2 and (b) 0.5. The full lines are the calculated curves, the open circles are the data points according to Refs. 9 and 27. The different curves for the specific-heat correspond to different Pade approximations.

with the fit for J_2. Combining the trends for both specific-heat and susceptibility data, the best fit for the materials gives (J_1/J_2, J_2, g) of (0.5, 3.9 K, 1.83).

Once again, to check the consistency of the experimental data with the LDA calculations, we show the best fits for the susceptibility data and the corresponding fit for the specific-heat data for $J_1/J_2=0.2$ (upper panel of Fig. 6) and $J_1/J_2=0.5$ (lower panel of Fig. 6). Although the latter ratio gives a better fit, both fits look reasonable and show that the LDA derived exchange constants give a good description of the material.

Summarizing this section, HTE and LDA derived exchange parameters that agree qualitatively quite nicely, characterizing both compounds as large J_2/J_1 systems with the ratio J_2/J_1 about twice as large in Li_2VOSiO_4 as in Li_2VOGeO_4. Due to the insensitivity of the HTE fits to the thermodynamical data and the remaining uncertainty in the LDA derived constants (uncertain value of U, possible ferromagnetic contributions), a more accurate determination of all the exchange constants requires more sensitive methods such as the measurement of the spin-wave dispersion by neutron scattering (see Sec. VII).

V. THREE-DIMENSIONAL ORDER

We now turn to the interplane couplings and the measurements of the Néel temperature, T_N, where three-dimensional order sets in. Applying the expression[15] $T_N \approx 0.36 J_\perp \xi^2(T_N)$ (ξ is the in-plane correlation length, and for small J_1 we ignore correlations between sublattices and treat the planes via a nearest-neighbor model), to our LDA calculated exchange constants, leads to the estimate $T_N \approx 3.6 \pm 0.4$ K for Li_2VOSiO_4, which is remarkably close to the experimental value of 2.8 K. For Li_2VOGeO_4, we would predict a slightly smaller transition temperature of $T_N \approx 3.2 \pm 0.4$ K derived from the LDA coupling constants. Considering our J_2 results from the best HTE fits (combining susceptibility and specific-heat) and the interplane exchanges $J_\perp$ from Table II, we find $T_N \approx 2.5 \pm 0.4$ K and $T_N \approx 1.7 \pm 0.4$ K for Li_2VOSiO_4 and Li_2VOGeO_4, respectively, again close to the experimental value for Li_2VOSiO_4. Although, no phase transition down to 1.9 K for Li_2VOGeO_4 was reported in Ref. 9, the specific-heat data[27] show a rather sharp peak with an onset at about 2.3 K (see inset in Fig. 6). Further experimental study to investigate the nature of this peak—proving or disproving our prediction of a phase transition to a columnar ordered phase at about this temperature—would be very interesting.

Furthermore, the saturation field for our calculated exchange constants in Li_2VOSiO_4 is about 30 T, which is much bigger than the 9 T field applied by Melzi *et al.*[28] The Néel temperature should go to zero at the saturation field. However, we note that due to suppression of spin fluctuation, the Néel temperature can increase slightly with field, as happens in the purely 2D model. Thus, the experimental result of very weak-field dependence of the Néel temperature up to 9 T is consistent with our expectations. The appreciable but still small 3D couplings should also give rise to 3D critical behavior at the finite-temperature transition with strong crossover effects. These results on the field dependence of the Néel temperature and the critical behavior at the transition in weakly coupled Heisenberg systems deserve further theoretical attention.

One of the really puzzling aspects of the experimental results[10] for Li_2VOSiO_4 is the small moment of 0.24 μ_B (extrapolated to $T=0$) obtained from the nuclear magnetic resonance split patterns, compared to the moment of the square-lattice Heisenberg model which is well known to be $\approx 0.6 \mu_B$.[14] One possible explanation, a partial cancellation of the hyperfine fields from antiferromagnetically ordered NN and NNN V sites, was given in Ref. 11. The arguments given there would be valid as well for the Li_2VOGeO_4 compound with a slightly smaller compensation. A more direct measurement of the ordered moments, for instance by neutron scattering, would be highly desirable to settle this point.

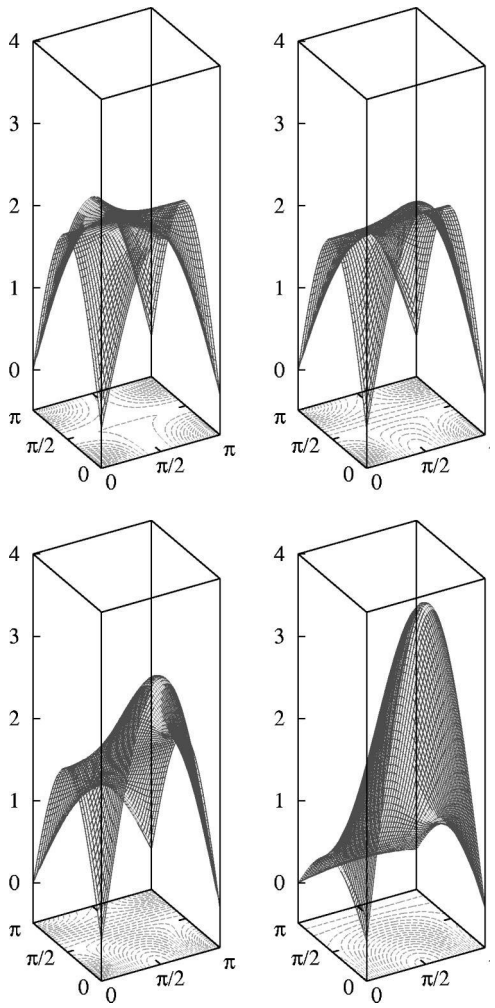

FIG. 7. Spin-wave spectra over the entire Brillouin zone for $J_1/J_2=$(a) 0.1, (b) 0.2, (c) 1.0, and (d) 1.9. The contours of constant energy are shown by dashed lines.

VI. SPIN-WAVE DISPERSION: SENSITIVE TESTS OF J_1/J_2 RATIO

We have seen in this paper that the materials Li_2VOSiO_4 and Li_2VOGeO_4 are good realizations of the quasi-2D frustrated antiferromagnets, where J_2 exceeds J_1. The LDA calculations lead to J_2 much larger than J_1. The ratio J_1/J_2 cannot be accurately determined from the available data primarily because the thermodynamic measurements are not very sensitive to its value. For this, we need to turn to the spin-wave dispersion.

The spin-wave dispersion for the J_1-J_2 model has been calculated by several authors. Let $\eta=J_1/2J_2$, $c_x=\cos q_x a$, and $c_y=\cos q_y a$ then in the collinear phase at low temperature, the spin-wave dispersion, to leading order in $1/S$, is given by[4,29]

$$\omega_\eta(\vec{q})^2=(2SJ_2)^2\{[1+\eta c_x]^2-[c_x c_y+\eta c_y]^2\}. \quad (10)$$

In this phase, the excitations are gapless at four points $\vec{q}=(0,0)$, $\vec{q}=(\pi,0)$, $\vec{q}=(0,\pi)$, and $\vec{q}=(\pi,\pi)$. This remains true throughout the phase $0<\eta<1$. However, the nature of the dispersion in the zone changes qualitatively as one goes from small η to η close to one. Two of the most notable features are illustrated in Fig. 7: (i) For small η, the dispersion is nearly symmetric in q_x and q_y, but as η approaches unity, the dispersion becomes highly asymmetric. This asymmetry reflects the antiferromagnetic order in one direction and ferromagnetic in the other. (ii) For small η, the spin-wave velocities are set by J_2 and the dispersion rises steeply and nearly isotropically around the gapless points, however, as one approaches $\eta=1$, the spin-wave velocity becomes very different along q_x and q_y and one sees an approach to lines of gapless states. The asymmetry in the spin-wave dispersion can be used as a measure of η.

Further, experimental work through neutron scattering would help determine the spin-wave spectra and the ratio J_1/J_2.

VII. CONCLUSIONS

In conclusion, this paper had two primary goals: (i) Presentation of high-temperature expansion results for the uniform susceptibility and specific heat of the J_1-J_2 square-lattice Heisenberg model. These results were augmented by perturbative mean-field theory valid for small J_1/J_2. With a growing number of experimental systems, which may be described well by the J_1-J_2 model, these expansions should prove useful in analyzing their experimental properties. (ii) We have presented first-principles calculations for the exchange constants of the materials Li_2VOSiO_4 and Li_2VOGeO_4 and by comparing with their experimental properties, have shown that these materials are in the large J_2 regime. We have also noted that an accurate determination of the J_1/J_2 ratio for such materials could come from the measurement of spin-wave dispersion.

ACKNOWLEDGMENTS

We thank F. Mila, O.A. Starykh, and P. Carretta for discussions, and P. Carretta for also providing us with the susceptibility and specific-heat data. This work was supported by the DAAD (individual grant H.R.), the NSF Grants Nos. DMR-0114818 and DMR-9986948, and by the Australian Research Council.

*Corresponding author. Email address: rosner@cpfs.mpg.de

[1] L. Capriotti, F. Becca, A. Parola, and S. Sorella, Phys. Rev. Lett. **87**, 097201 (2001).

[2] O.P. Sushkov, J. Oitmaa, and Zheng Weihong, Phys. Rev. B **63**, 104420 (2001).

[3] E. Shender, Sov. Phys. JETP **56**, 178 (1982).

[4] P. Chandra, P. Coleman, and A.I. Larkin, Phys. Rev. Lett. **64**, 88 (1990).

[5] P. Chandra and B. Doucot, Phys. Rev. B **38**, 9335 (1988).

[6] R.R.P. Singh, Zheng Weihong, C.J. Hamer, and J. Oitmaa, Phys. Rev. B **60**, 7278 (1999).

[7] P. Carretta, N. Papinutto, C. B. Azzoni, M. C. Mozzati, E. Pa-

varini, S. Gonthier, and P. Millet, Phys. Rev. B **66**, 094420 (2002).
[8] E. E. Kaul, C. Geibel, A. V. Mironov, R. V. Shpanchenko, and E. V. Antipov, E-Verhandlungen der DPG 2002, TT 5.2, 2002.
[9] R. Melzi, P. Carretta, A. Lascialfari, M. Mambrini, M. Troyer, P. Millet, and F. Mila, Phys. Rev. Lett. **85**, 1318 (2000).
[10] R. Melzi, S. Aldrovandi, F. Tedoldi, P. Carretta, P. Millet, and F. Mila, Phys. Rev. B **64**, 024409 (2001).
[11] H. Rosner, R.R.P. Singh, W.H. Zheng, J. Oitmaa, S.-L. Drechsler, and W.E. Pickett, Phys. Rev. Lett. **88**, 186405 (2002).
[12] H.X. He, C.J. Hamer, and J. Oitmaa, J. Phys. A **23**, 1775 (1990); M.P. Gelfand, R.R.P. Singh, and D.A. Huse, J. Stat. Phys. **59**, 1093 (1990).
[13] See for example, A. J. Guttmann in *Phase Transitions and Critical Phenomena*, edited by C. Domb and J. Lebowitz (Academic, New York, 1989), Vol. 13.
[14] C.J. Hamer, Zheng Weihong, and J. Oitmaa, Phys. Rev. B **50**, 6877 (1994); R.R.P. Singh, *ibid.* **39**, 9760 (1989).
[15] S. Chakravarty, B.I. Halperin, and D.R. Nelson, Phys. Rev. Lett. **60**, 1057 (1988).
[16] J.K. Kim and M. Troyer, Phys. Rev. Lett. **80**, 2705 (1998).
[17] N. Elstner *et al.*, Phys. Rev. Lett. **75**, 938 (1995).
[18] D.J. Scalapino, Y. Imry, and P. Pincus, Phys. Rev. B **11**, 2042 (1975).
[19] P. Millet and C. Satto, Mater. Res. Bull. **33**, 1339 (1998).
[20] K. Koepernik and H. Eschrig, Phys. Rev. B **59**, 1743 (1999).
[21] J.P. Perdew and A. Zunger, Phys. Rev. B **23**, 5048 (1981).
[22] H. Eschrig, *Optimized LCAO Method and the Electronic Structure of Extended Systems* (Springer, Berlin, 1989).
[23] K. Held, G. Keller, V. Eyert, D. Vollhardt, and V.I. Anisimov, Phys. Rev. Lett. **86**, 5345 (2001).
[24] T. Mizokawa and A. Fujimori, Phys. Rev. B **48**, 14 150 (1993); J. Zaanen and G.A. Sawatzky, J. Solid State Chem. **88**, 8 (1990).
[25] The specified error results from the uncertainity of U and the errors for t_1 and t_2 from the tight-binding fit.
[26] Zheng Weihong, C.J. Hamer, and J. Oitmaa, Phys. Rev. B **60**, 6608 (1999).
[27] R. Melzi, Ph.D. thesis, University of Pavia, 2002; P. Carretta *et al.* (unpublished).
[28] We note that if we take our fitted value of $J_2 = 6.1$ K, the Néel temperature estimate will become ≈ 2.6 K and the saturation field ≈ 20 T.
[29] A.F. Barabanov and O.A. Starykh, JETP Lett. **51**, 311 (1990).